AIAA JOURNAL
Vol. 49, No. 6, June 2011

Instantaneous De-Icing of Freezer Ice via Ultrasonic Actuation

Jose Palacios,* Edward Smith,† and Joseph Rose‡
Pennsylvania State University, University Park, Pennsylvania 16802
and
Roger Royer§
FBS Worldwide, Inc., State College, Pennsylvania 16803

DOI: 10.2514/1.J050143

A low-power, nonthermal, ultrasonic de-icing system is introduced as a potential de-icing system for helicopter rotor blades. In this research effort, ultrasonic actuators excite isotropic plates and airfoil-shaped structures that are representative of helicopter leading-edge protection caps. The system generates delaminating ultrasonic transverse shear stresses at the interface of accreted ice, debonding thin ice layers (less than 3 mm thick) as they form on the isotropic host structure. A finite element model of the proposed actuator and the isotropic structures with accreted ice guides the selection of the actuator prototypes. Several actuator-isotropic plate structures are fabricated and tested under freezer ice conditions. Test results demonstrate that radial resonance disk actuators (28–32 kHz) create ultrasonic transverse shear stresses capable of instantaneously delaminating ice layers. The finite element modeling predicts the delamination patterns of the accreted ice layers. Models also predict (within 15%) the required input voltage to promote instantaneous ice debonding. At environment temperatures of −20°C, the system delaminates 2.5-mm-thick ice layers with power input densities as low as 0.07 W/cm^2 (0.5 W/in.^{2}).

Nomenclature

A = ice area, m^2
c^E = elastic stiffness at constant electric field, N/m^2
D = electric displacement vector, C/m^2
E = applied external electric field vector, V/m
e = piezoelectric coupling, N/(m V)
F = applied mechanical force, N
F_s = shear force, N
I = current, A
K_{uu} = elastic stiffness matrix, N/m
$K_{u\varphi}$ = piezoelectric stiffness matrix, N/V
$K_{\varphi\varphi}$ = dielectric matrix, F
M = mass matrix, kg
Q = vector of the nodal charges, C
Q_P = piezoelectric heat generation per unit volume, W/m^3
S = strain vector
T = stress vector, N/m^2
T_0 = bottom surface host-structure temperature, °C
T_1 = lead zirconate titanate and host-structure interface temperature, °C
T_2 = lead zirconate titanate surface temperature, °C
U = elastic displacement, m
Z = impedance, Ω
α = thermal conductivity, W/m K
ε^S = dielectric stiffness at constant strain, F/m
θ = phase, rad
σ_{XY} = shear stress, N/m^2
σ_{ZX} = transverse shear stress, N/m^2
Φ = electric potential, V
φ = electric potential, V
Ω = piezoelectric boundary condition domain
ω = frequency, rad/s

Received 19 August 2009; revision received 19 January 2011; accepted for publication 24 January 2011.

*Research Associate, Department of Aerospace Engineering, 229 Hammond Building. Member AIAA.
†Professor Aerospace Engineering, 231D Hammond Building. Member AIAA.
‡Paul Morrow Professor, Engineering Science and Mechanics, 0212 Earth and Engineering Sciences. Member AIAA.
§Director of Technology and Business Development, 143 Hawbaker Industrial Drive, Suite 102.

I. Introduction

WATER particles freeze on impact with the leading edge of the rotor blade when a combination of temperatures close to freezing, high speeds, and high cloud water concentrations occur [1]. Both helicopter and tiltrotor blades operating at temperatures below freezing tend to collect ice along the majority of the leading edge of the blade [2]. As ice accumulation alters the stagnation-point geometry of the blade, the performance of the vehicle decreases. Rotor ice adhesion increases drag, promotes flow separation, and introduces high vibration levels. The increase in drag generated by accreted ice increases the torque required to maintain the lift of the vehicle.

Scavuzzo et al. [3] modeled and demonstrated that ice shedding is another major problem introduced by ice accretion on rotating blades. Shear stresses at the interface between ice and the leading edge of the airfoil increase linearly with ice thickness due to centrifugal forces acting on the ice layer. When the shear stresses exceed the ultimate adhesive shear strength of the ice, shards of ice are released. The impact of shed ice could cause serious damage to the aircraft. If ice sheds unevenly, rotor mass unbalance introduces undesired vibrations and changes the handling of the vehicle.

To avoid critical ice formation on the rotor, industry has adopted a standard de-icing system for a limited number of helicopter models. This de-icing system uses thermal energy to melt accreted ice. The thermal de-icing mechanism is only run periodically to avoid large power consumption or excessive heating of the leading-edge structure. The ice thickness can reach up to 1 cm before the thermal system debonds the accreted ice. Such a system requires large amounts of energy (∼3.9 W/cm^2 or 25 W/in.^{2}) and contributes to an undesired increase in the overall weight and cost of the blade. Melted ice might flow in the aft direction to refreeze. Released ice patches are also a ballistic concern. Because of these drawbacks, many small and medium size civil helicopters do not employ any de-icing capabilities, limiting the operations of these vehicles under adverse conditions.

The quest for a low-power, nonthermal de-icing system has generated several impulsive de-icing systems that aim to crack and

shed off accreted ice. Electroimpulsive ice protection systems [4], electromagnetic impulsive-eddy current repulsion [5], pneumatic inflation [2,6], shape memory alloy stresses and structural resonance [7,8], and fluid anti-icing [2] are some of the de-icing methods that have been studied. Power reduction and nonthermal ice removal was accomplished by these proposed systems, but each of them has related drawbacks. Electroimpulsive de-icing has never been applied to helicopter rotor blades due to the large volume of the actuation, fatigue stress considerations, and related challenges for implementation in the finite D-spar space. Pneumatic inflation was shown to erode when placed on the leading edge of a helicopter blade. Detached ice impact concerns remained with pneumatic leading-edge de-icing. Structural resonance systems also required ice to accrete to considerable thickness. In addition, the stresses created by the vibration in the blade are a concern for D-spar composite delamination. Fluid anti-icing requires large amounts of fluid to be carried on board. The de-icing fluid has to be transferred to the blades via complicated slip rings. In addition, leading-edge orifice clogging is a concern for this type of system.

Ramanathan et al. [9] proposed the use of ultrasonic shear waves as a low-power ice protection system. In his research, a 1 MHz shear mode piezoelectric patch was applied to an isotropic plate with a layer of ice. Ice-interface melting slowly took place and approximately 100 s after the actuator was turned on, the ice patch delaminated. Venna et al. described similar melting patterns at lower excitation frequencies (1000 Hz) that introduced localized high stress due to resonating piezoelectric actuators [7]. Palacios et al. [10] also observed melting of accreted ice layers under the effects of ultrasonic shear vibration. The accreted ice layers showed instantaneous microscopic ice cracking and melting with resonating piezoelectric shear actuators (130 kHz). Heat propagation from the actuator, as a major source of energy melting the ice interface, is a concern for all the high-frequency vibration research mentioned above. Heat propagation as the main source for ice removal presents challenges when combined with new leading-edge highly-erosion-resistant polymer-based materials. The lower thermal propagation properties of these materials introduce melting concerns.

The experimental results obtained in above mentioned ultrasonic/vibration research efforts did not demonstrate instantaneous ice delamination despite predicting interface shear stresses exceeding the adhesion strength of the substrate. A summary of these results related to ultrasonic/vibration de-icing is summarized in Table 1.

In addition to active de-icing systems, passive systems such as ice-phobic surfaces are also being investigated as potential solutions to ice accretion. Ice-phobic materials have not shown, to date, the ability to withstand erosion environments representative of rotorcraft vehicles. These ice-phobic materials degrade under rain and sand erosion environments losing their ice-phobic properties.

A new approach to use piezoelectric actuators to cause *instantaneous* ice delamination is described in this paper. Taking advantage of the low shear adhesion strength of ice, ultrasonic piezoelectric actuators demonstrate the capability of delaminating thin ice layers (<3 mm) without any time delay after the actuator is turned on. Centrifugal forces introduced on accreted ice layers during rotor operation in icing conditions will reduce required interface stresses. Instantaneous ice delamination occurs while the actuator temperature remains well under freezing temperatures, eliminating heat propagation as the main source of ice debonding.

The objectives of the research presented in this paper are 1) to develop a design procedure for the selection of ultrasonic de-icing actuators, 2) to present experimental results demonstrating instantaneous delamination of freezer ice, and 3) to correlate these results with predictions. Predictions of the transverse shear stresses between an isotropic host structure and an accreted ice layer under the effects of ultrasonic vibration were performed using finite element analysis. All the proof-of-concept experiments presented in this paper were conducted with freezer ice.

II. Ice Adhesion Strength Measurement

Extensive work to experimentally determine the adhesion strength of ice to different materials and under different icing conditions has been conducted by multiple authors [3,12–16]. Ramanthan et al. [9] and Venna et al. [7] presented literature reviews on the subject. Based on the experimental shear adhesion strength measurements between ice and steel that were presented in the referenced literature, the expected shear adhesion strength value of refrigerated glaze ice can be expected to range between 0.24 and 1.7 MPa. Some authors present lower shear adhesion strengths for wind-tunnel impinging ice than freezer ice, but there are also arguments stating that the opposite is true [7]. The large ice shear adhesion strength discrepancies are believed to be due to differences on material used, surface roughness, water purity, and ice accretion conditions (freezer, rime, and glaze ice) between the different tests reported in the literature. Because of this large ice shear adhesion strength discrepancies, an ice adhesion measurement rig, was fabricated to experimentally measure the shear adhesion strength of ice to the stainless steel material (grade 430) used in this research for demonstration of instantaneous ultrasonic de-icing. A photograph and schematic of the ice adhesion strength measurement rig is depicted in Fig. 1. The rig was used to measure the shear adhesive strength of freezer ice bonded to steel plates that were used in this research.

A shear force F_s applied a known stress to an ice patch with a given surface area A. A high-traction surface was frozen on top of the accreted ice patch. The high-traction surface was connected to a cable-pulley mechanism that transformed vertical weight forces to horizontal shear forces on the ice patch. To ensure steady-state conditions in the ice adhesion strength during each test, the ice patches were allowed to freeze for 5 h (Fig. 2).

The force responsible for ice delamination was used to calculate the adhesion strength of the ice, as presented in Fig. 1:

$$\sigma_{ZX} = \frac{F_s}{A} \tag{1}$$

The surface to which the ice adheres was polished with a 10-μm-grain sandpaper, followed by antigrease and acetone to avoid surface contamination and to ensure proper ice adhesion. Because surface roughness is a critical factor determining ice adhesion, a digital profilometer was used to experimentally measure the surface roughness of the metal (± 2.14 μm, Fig. 3). The average adhesion shear strength of freezer ice to steel at -10°C was experimentally measured to be 1.5 MPa. The maximum shear adhesion strength of ice to steel found by Raraty and Tabor [14] is 1.66 MPa.

III. Actuator Selection and Modeling

To demonstrate instantaneous ice delamination due to ultrasonic excitation, a suitable actuator, able to provide transverse shear stresses exceeding the adhesion strength of ice to steel, has to be selected. To eliminate thermal energy as the main cause of ice debonding, the temperature of the actuator should remain well below freezing when continuously driven at a suitable de-icing ultrasonic

Table 1 Vibration de-icing observations [7,9,10]

Author	Structure	Actuation mode	Frequency, kHz	Ice type, temp °C	Shear stress, MPa	Time before debonding, s
Lemont and Upton [11]	Rotor blade	Bending and torsion	$0–5 \times 10^{-4}$	Glaze	Unknown	2
Venna et al. [7]	Airfoil shape	Shear and longitudinal	1	Freezer (−15 to −6)	∼7.5	∼127
Ramanathan et al. [9]	Flat plate	Shear	$\sim 1.1 \times 10^3$	Freezer (−20)	∼1	∼170
Palacios et al. [10]	Flat plate	Shear	130	Freezer (−20)	∼10	∼110

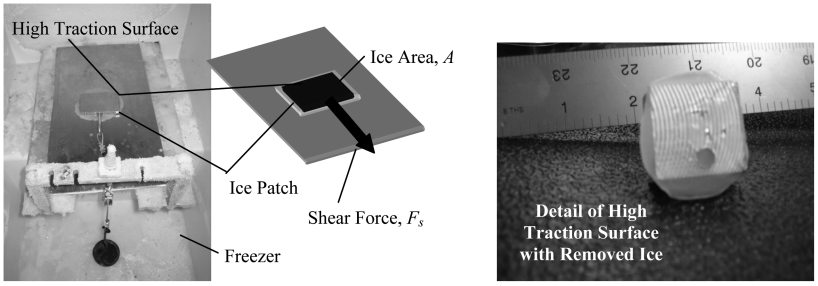

Fig. 1 Photograph and schematic of the ice adhesion measurement rig and detail of high-traction surface.

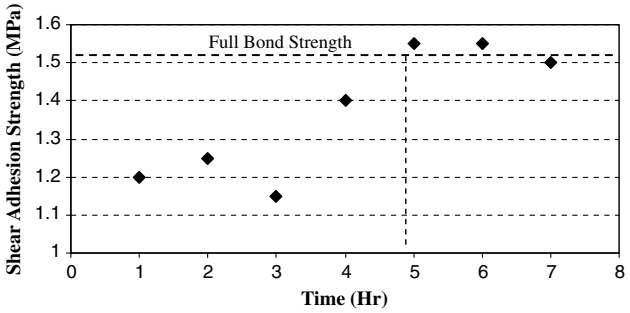

Fig. 2 Ice adhesion strength vs freezing time. steady adhesion strength is reached 5 h after water is placed on a steel surface.

frequency. Three critical parameters to demonstrate ultrasonic instantaneous ice delamination are required: impedance matching between the actuator and the driving electronics, the capability of the ultrasonic actuator to generate the required ice-interface stresses, and the ability of the actuator to remain under freezing conditions when driven at the required frequency and input voltage to promote instantaneous ice delamination.

A. Impedance Matching

In prior research described in [10] regarding the effects of ultrasonic vibration on ice accretion, instantaneous ice debonding was not experimentally observed despite predicted ultrasonic transverse shear stresses exceeding the static adhesion strength of the ice layer. The lack of instantaneous ice debonding observed in the results is explained by the lack of impedance matching during the experiments. Impedance matching refers to the practice of attempting to make the output impedance of the power source equal to the input impedance of the actuator to which it is ultimately connected to. This is done to maximize the power transfer and minimize reflections from the load. Impedance matching is a partial solution to minimize input power requirements to generate sufficient ice-interface stresses to debond accreted ice. The forward power is denoted as the power sent to the actuator systems, while the backward power is that power reflected from the system. To ensure that the voltage reaching the actuator is effectively being converted into mechanical energy, minimum backward (or reflected) power is

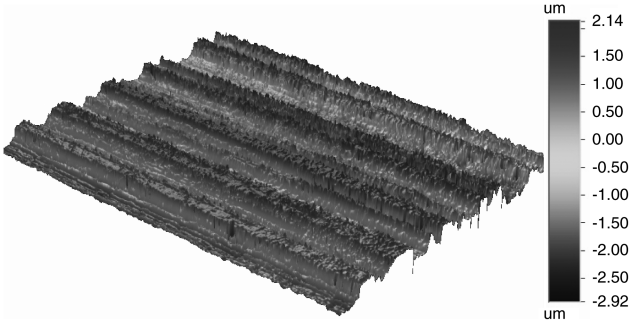

Fig. 3 Grade-430 stainless steel surface roughness measured with a digital profilometer.

desired. To create this condition, impedance matching between the source (amplifier) and the load (actuator system) must occur at ultrasonic mode frequencies. This requirement is expressed by Eq. (2), where Z_L is the impedance of the load and Z_S is the impedance of the source:

$$Z_L = Z_S \tag{2}$$

The derivation of this requirement is found in [17].

Electrical impedance describes a measure of opposition to a continuous sinusoidal alternating current. Electrical impedance provides information on the relative amplitudes and relative phase of the voltage potential and current in an alternating circuit. Complex impedance is defined as the ratio of these quantities:

$$\tilde{Z} = \frac{\tilde{\varphi}}{\tilde{I}} \tag{3}$$

In a direct current circuit there is no distinction between impedance and resistance. The symbol for impedance is usually Z. θ is the phase of the impedance. Impedance is represented as a complex quantity, $\tilde{Z}$, as shown in Eq. (4):

$$\tilde{Z} = Ze^{j\theta} \tag{4}$$

where the magnitude Z represents the ratio of the voltage amplitude to the current amplitude. The argument θ gives the phase difference between voltage and current.

The meaning of electrical impedance can be understood by substituting it into Ohm's law [Eq. (5)]:

$$\tilde{\varphi} = \tilde{I}\,\tilde{Z} = \tilde{I}Ze^{j\theta} \tag{5}$$

The magnitude of the impedance Z acts as a resistance, giving the drop in voltage amplitude across an impedance value $\tilde{Z}$ for a given current $\tilde{I}$.

The actuator must have an impedance value at the selected ultrasonic mode (mode able to create sufficient interface stresses to delaminate accreted ice) such that is similar to that of the driving electronics, formed by an amplifier and a signal generator. An impedance matching network able to vary the electronic impedance between 25 and 400 Ω was used in this research. This network is part of an ultrasonic amplifier (AR 800) with a frequency bandwidth ranging from 10 kHz to 3 MHz.

B. Ice-Interface Transverse Shear Stress

To select an ultrasonic actuator able to instantaneously delaminate accreted freezer ice, it is important to not only ensure impedance matching between the actuator and the amplifier source, but to also provide interface shear stresses exceeding the adhesion strength of the accreted ice. There are two different types of interface shear stresses created on the host structure under the actuation of a piezoelectric material: ZX transverse shear stresses and XY shear stresses. ZX transverse stresses are surface stresses, and are zero at free traction surfaces, while XY shear stresses can be nonzero throughout a finite element thickness. ZX stresses introduced at the ice–host-structure interface are responsible for delamination processes between layers, while XY shear stresses contribute to ice cracking. A schematic of referred stresses is illustrated in Fig. 4.

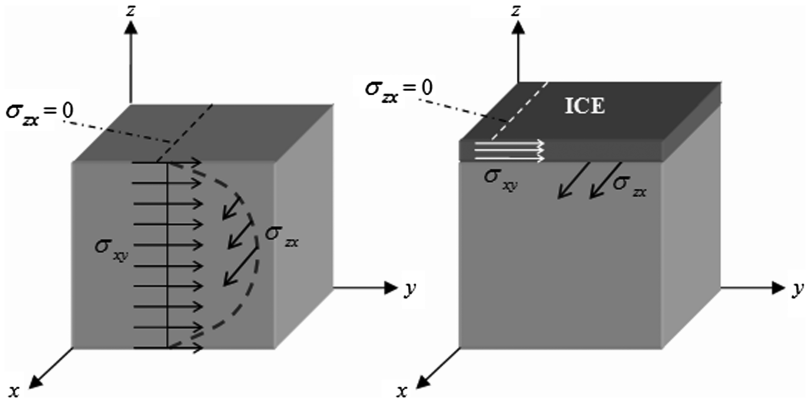

Fig. 4 Stresses σ_{zx} is zero at the elements free traction surfaces, but promotes delamination between a host structure and accreted ice layer. The ice layer will also undergoes σ_{xy} stresses through its thickness (stresses responsible for ice cracking).

When ice accretes, the surface of the host structure is no longer free of tractions, and *XY* stresses as well as *ZX* stresses are present at the ice interface. The delamination process induced by *ZX* transverse shear stresses is explained by Jones [18]. As the transverse shear stresses exceed the shear adhesion strength of ice, ice delamination is predicted.

When the *XY* shear stresses exceed the shear strength of ice, ice fracture occurs. Determining the shear strength of ice under ultrasonic strains is beyond the scope of this work, since instantaneous ice debonding under ultrasonic vibration (high interface *ZX* transverse shear stresses) is the main objective of this research effort.

C. Finite Element Modeling

A commercial finite element package was used to model different lead zirconate titanate (PZT) actuators attached to a 0.7-mm-thick, 30.5 cm × 30.5 cm steel plate. A summary of the constitutive and equilibrium equations used by the software is presented below.

Piezoelectric effects occur in noncentrosymmetric crystals, such as PZT and quartz. Electric dipoles are generated due to mechanical deformations. The converse effect (reverse piezoelectric effect) has been used in this research to generate transverse shear stresses between a host structure and ice in order to debond the freezer ice.

The following summarized finite element method derivation is described in detail in [19–22]. The constitutive equations for piezoelectric materials under small field conditions are defined in Eq. (6):

$$T_{ij} = c^E_{ijkl} S_{kl} - e_{kij} E_K \qquad D_i = e_{kij} S_{kl} + \varepsilon^S_{ij} E_j \tag{6}$$

where D is the electric displacement vector (C/m^2), S is the strain vector, E is the applied external electric field vector (V/m), and T is the stress vector (N/m^2). The elastic stiffness at constant electric field, c^E, the piezoelectric coupling, e, and the dielectric stiffness at constant strain, ε^S, are assumed to be constant, which is a reasonable assumption for piezoelectric materials subjected to moderate electric fields (and therefore small deformations).

Newton's law must be verified [Eq. (7)] for a uniform assumed displacement [Eq. (8)]:

$$\rho \frac{\partial^2 u_i}{\partial t^2} = \frac{\partial T_{ij}}{\partial x_j} \tag{7}$$

$$u = U(x, \omega) e^{i\omega t} \tag{8}$$

The change of the electric displacement vector D must be equal to zero when no macroscopic charges are present in the medium [Gauss's theorem, Eq. (9)]. In addition, considering small deformations, the strain tensor S can be written as shown in Eq. (10). Finally, assuming electrostatic conditions, the electrostatic potential φ is related to the electric field E by Eq. (11):

$$\frac{\partial D_i}{\partial x_i} = 0 \tag{9}$$

$$S_{kl} = \frac{1}{2}\left(\frac{\partial u_k}{\partial x_l} + \frac{\partial u_l}{\partial x_k}\right) \tag{10}$$

$$E_i = -\frac{\partial \varphi}{\partial x_i} \tag{11}$$

The constitutive equations for PZT materials can be rewritten as follows:

$$-\rho\omega^2 u_i = \frac{\partial}{\partial x_j}\left(c^E_{ijkl} S_{kl} - e_{kij} E_K\right) \qquad \frac{\partial}{\partial x_j}\left(e_{kij} S_{kl} + \varepsilon^S_{ij} E_j\right) = 0 \tag{12}$$

Mechanical boundary conditions can be established by assuming Dirichlet conditions apply for the displacement field such that

$$u_i = u_0 \tag{13}$$

and where u_0 is a known vector. S_u is the strain matrix with surface of elements subjected to this condition.

Similarly, the stress field must fulfill Neumann condition [Eq. (14)], and for convenience, the ensemble of surface elements subjected to this condition is labeled as S_T. The vector n, normal to the boundaries of the system defining the domain Ω, relates the strain tensor and a known vector f^0, as follows:

$$T_{ij} \cdot n_j = f^0_i \tag{14}$$

Electrical boundary conditions dictate that those surfaces not covered by electrodes must be free of surface charges, since no electric fields are applied on those surfaces. This is represented by Eq. (15):

$$D_i \cdot n_i = 0 \tag{15}$$

For those surfaces with electrodes the excitation on the pth electrode (there are p electrodes in the system), the charge on the electrode is defined by

$$-\iint_{S_p} D_i n_i \, \mathrm{d}S_P = Q_P \tag{16}$$

The variation principle is used to define the functional over the domain and its boundaries. Using the system of equations and boundary conditions defined above, a functional, Π, where the mechanical and electrical energy of the system (terms integrated in the domain Ω) are defined is identified [Eq. (17)]:

$$\prod = \iiint_{\Omega} \frac{1}{2}(S_{ij} c^E_{ijkl} S_{kl} - \rho\omega^2 u_i^2)\,\mathrm{d}\Omega - \iint_{S_u} (u_i - u_i^0) n_j (c^E_{ijkl} S_{kl} - e_{kij} E_K)\,\mathrm{d}S_u - \iint_{S_T} f_i u_i\,\mathrm{d}S_T - \iiint_{\Omega} \frac{1}{2}(2 S_{kl} e_{ikl} E_i + E_i \varepsilon^S_{ij} E_j)\,\mathrm{d}\Omega - \sum_{P=0}^{P} \iint_{S_P} (\varphi - \varphi_p) n_i (e_{ikl} S_{kl} + \varepsilon^S_{ij} E_j)\,\mathrm{d}S_P + \sum_{P=0}^{P} \varphi_p Q_P \tag{17}$$

The above functional can be rewritten in terms of finite elements by applying finite element methods. The finite element method determines an approximate solution of the form

$$w \approx \hat{w} = \sum N_i a_i \tag{18}$$

where N_i are acceptable shape functions that guarantee the continuity of the geometry between elements and that are prescribed in terms of independent coordinates. a_i are nodal parameters for the displacement, u, and electric potential fields, φ.

The solution functions of the piezoelectric problem can be rewritten in terms of shape functions such that for each element defined by n nodes, there is an electrical boundary condition, Ω^e, where the electric field can be written as

$$E = -B^e_{\phi} \Phi \tag{19}$$

where Φ is the vector of the nodal values of the electrostatic potential and

$$B^e_{\varphi} = \begin{bmatrix} \frac{\partial N^e_i}{\partial x} & \frac{\partial N^e_i}{\partial y} & \frac{\partial N^e_i}{\partial z} \end{bmatrix}^T \tag{20}$$

In the same fashion, for each element, the strain tensor is defined by Eq. (21), where U is the vector of the nodal values of the displacement:

$$S = -B^e_u U \tag{21}$$

$$B^e_u = \begin{bmatrix} \frac{\partial N^e_i}{\partial x} & 0 & 0 & 0 & \frac{\partial N^e_i}{\partial z} & \frac{\partial N^e_i}{\partial y} \\ 0 & \frac{\partial N^e_i}{\partial y} & 0 & \frac{\partial N^e_i}{\partial z} & 0 & \frac{\partial N^e_i}{\partial x} \\ 0 & 0 & \frac{\partial N^e_i}{\partial z} & \frac{\partial N^e_i}{\partial y} & \frac{\partial N^e_i}{\partial x} & 0 \end{bmatrix}^T \tag{22}$$

The general system of equations is rewritten as shown in Eq. (23), and U and Φ are the degrees of freedom of the finite element problem:

$$T = c^E B^e_u U + e^T B^E_{\varphi} \Phi \qquad D = e B^e_u U + \varepsilon_S B^e_{\varphi} \Phi \tag{23}$$

By performing the integration on the shape function matrices and their derivatives, the functional can be rewritten as

$$\Pi_e = (U^e)^T (K^e_{uu} - \omega^2 M^e) U^e + (U^e)^T K^e_{u\varphi} \Phi^e + \frac{1}{2}(\Phi^e)^T K^e_{\varphi\varphi} \Phi^e - (U^e)^T F^e + \sum_{p=0}^{P} \varphi_p Q_p \tag{24}$$

where, K_{uu}, $K_{\varphi u}$, and $K_{\varphi\varphi}$ are the elastic, piezoelectric and dielectric stiffness matrices, and M is the mass matrix:

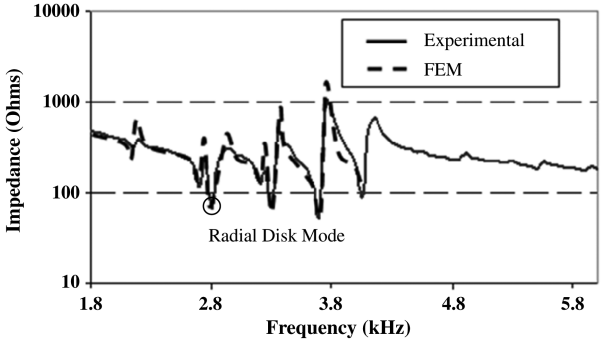

Fig. 6 Experimental and predicted impedance curves of the PZT-4 disk bonded to a 30.5 cm × 30.5 cm steel plate (FEM is the finite element method).

$$K^e_{uu} = \iiint_{\Omega^e} (B^e_u)^T c^E B^e_u\,\mathrm{d}\Omega^e \tag{25}$$

$$K^e_{\varphi u} = \iiint_{\Omega^e} (B^e_u)^T c^E B^e_{\varphi}\,\mathrm{d}\Omega^e \tag{26}$$

$$K^e_{\varphi\varphi} = \iiint_{\Omega^e} (B^e_{\varphi})^T \varepsilon^S B^e_{\varphi}\,\mathrm{d}\Omega^e \tag{27}$$

$$M^e = \iiint_{\Omega^e} \rho\omega^2 (N^e)^T N^e\,\mathrm{d}\Omega^e \tag{28}$$

$$F^e = \iint_{S^e_T} (N^e)^T f\,\mathrm{d}S^e_T \tag{29}$$

The application of the variational principle to the functional implies its minimization with respect to variations of the nodal values of U and Φ. From the stationary condition, and looking into the harmonic behavior of the system (reverse piezoelectric effect at various input frequencies), the following relation arises as Q (electrical excitation applied to the PZT material) is nonzero:

$$\begin{bmatrix} K_{uu} & K_{u\varphi} \\ K^T_{u\varphi} & K_{\varphi\varphi} \end{bmatrix} \begin{bmatrix} U \\ \Phi \end{bmatrix} = \begin{bmatrix} F \\ -Q \end{bmatrix} \tag{30}$$

Note that no forces are applied to the actuator; therefore, F is zero. Harmonic analysis is performed to calculate the impedance of the system at different frequencies. This analysis describes the response of the piezoelectric actuator/steel-plate/ice system due to an applied external electric potential to the PZT actuator at an angular frequency ω (φ applied to the electrodes). The electrical current entering the electrodes is written as $I = j\omega Q$. Therefore, the impedance, Z, of each electrode is given by the ratio φ/I. The frequency-dependent impedance values are used to determine the actuator-structure resonance frequency. Resonating ultrasonic modes occur at those frequencies where the ultrasonic actuator provides a maximum current output for a given driving voltage. The displacement and stress fields in the structure are calculated at any selected driving frequency.

A 7.6-cm-diam, 2.5-mm-thick PZT-4 disk was selected to impart in-plane stresses on the 0.7-mm-thick, 30.5 cm × 30.5 cm stainless

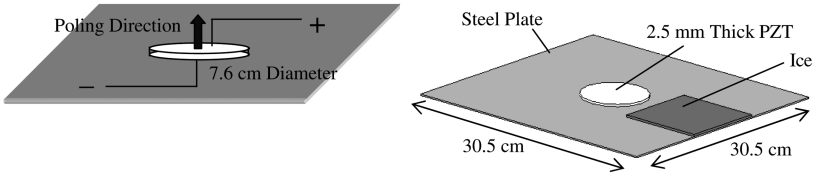

Fig. 5 Schematic of PZT-4 disk attached to a 30.5 cm × 30.5 cm × 0.71 mm steel plate.

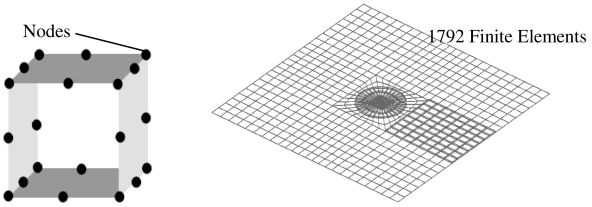

Fig. 7 20 Node 3-D finite element, and group of elements modeling a system formed by a steel plate, PZT disk, and isotropic ice layer.

steel plate. The ice thickness was selected to be 75% less than the maximum ice thickness that is allowed to accrete by electrothermal de-icing systems that are currently used in helicopter rotor blades [2]. This thickness would not create a ballistic concern, given its reduced inertia after shedding. A schematic and photograph of the structure is illustrated in Fig. 5.

The actuator was selected because the predicted impedance of the actuator attached to the host structure was calculated to be less than 400 Ω at those frequencies corresponding with impedance lows. This impedance value is in the range of the matching network of the power supply used during this research. Experimental and predicted impedance values agree with errors of less than 3% at impedance lows, as illustrated in Fig. 6.

Accreted ice layers were assumed to be isotropic and perfectly bonded to the steel plate (ice Young's modulus 9100 MPa, ice density 900 kg/m^3, and ice Poisson's ratio 0.3). The steel plate and the ice layers are modeled with 20-node 3-D quadratic isotropic elements, while the piezoelectric actuator is modeled using 20-node 3-D quadratic piezoelectric elements (Fig. 7).

Most important, the actuator was selected because, when driven at its ultrasonic radial mode (60 W input power, 28.5 kHz), it provided predicted transverse shear stresses at the interface of a 2.5-mm-thick ice layer that exceed the experimentally measured shear adhesion strength of ice to steel (1.5 MPa). Instantaneous ice debonding is predicted under these conditions when the sinusoidal input signal reaches a maximum. The *ZX* transverse shear stresses generated at the ice interface were calculated to reach up to 2 MPa at the interface of a 2.5-mm-thick ice layer when driven at mentioned conditions. The ice-interface transverse shear stresses for different frequencies are shown in Table 2. The maximum ice-interface shear stress is identified for the ultrasonic mode occurring at 28.5 kHz. The predicted transverse shear stresses results, calculated for a maximum of the continuous input excitation, are illustrated in Fig. 8.

Note that the stresses at the interface of the actuator and the steel plate, depicted in Fig. 8, are comparable with those created at the ice interface. For this reason, a bond with adhesion strength exceeding that of the ice was selected. The PZT-4 disks were bonded to the steel-plate structure using Eccobond 286, glue used for high-frequency applications with a thermal bandwidth ranging from −40°C up to 200° C and shear adhesion strength to steel of 20 MPa. The bonding layer was not modeled in the finite element analysis.

D. Thermal Modeling and Experimental Correlation

Actuator heating is the final selection parameter required to demonstrate instantaneous ice delamination due to ultrasonic ice-interface transverse shear stresses. Elastic, dielectric, and piezoelectric losses degrade the performance of the PZT actuators as described in [23,24]. Electrical energy supplied to the PZT actuators to drive the host structure is transformed not only into mechanical motion (dictated by the coupling factors of the material), but also into internal heat that is transferred to the host structure. Damping in the actuator and dielectric losses create distributed heat generation in the PZT material and the host structure. Temperature increases in the system facilitate ice melting and generate additional thermal stresses. To minimize these effects, a PZT actuator with temperature increases not exceeding freezing is sought. Following the theoretical model presented in [23] and summarized by Eq. (31), heat generation estimates were performed to calculate the temperature increase of potential PZT actuator for predicted input power and resonance frequencies required to promote instantaneous ice delamination. Ensuring that the actuator would not exceed freezing temperatures eliminates thermal effects as the main source responsible for ice debonding:

Table 2 Ice-interface transverse shear stress amplitude vs frequency, 50 V sine wave input

Frequency, kHz	Impedance, Ω	Ice-interface transverse shear amplitude, MPa
18	480	0.0015
28.5	65	2.0
33	70	0.5
37	56	1.2

$$T_{\max} = T_1 + \left[\frac{1}{2} + \frac{\alpha_p}{Q_p}\frac{T_2 - T_1}{(z_2 - z_1)^2}\right]\left[\frac{1}{2}(T_2 - T_1) + \frac{Q_p}{\alpha_p}\frac{(z_2 - z_1)^2}{4}\right] \tag{31}$$

where Q_p, is the heat generation rate per unit volume in the PZT actuator,

$$Q_p = \frac{\text{power}}{\text{volume}} = \frac{P_p}{V} \tag{32}$$

and where the dissipative power consumption of the material, P_p, is

$$P_p = \frac{V^2}{2Z} \tag{33}$$

The interface temperature and the maximum actuator temperature of a PZT-4 disk bonded to a 0.71-mm-thick steel plate was theoretically calculated and compared with experimental results. The freezer environment temperature was maintained at −10°C. The temperature of the surface of the plate and disk was measured before turning the actuator on. The recorded temperatures were used as boundary conditions for the thermal governing equation described in [25]. Different input ultrasonic frequencies excited the 45.6 cm^2 disk actuator. The input voltage was 50 V (27.8 KV/m). The impedance at each different frequency was experimentally measured and can be seen in Fig. 6. From the impedance of the actuator and the input voltage, the power dissipation was calculated.

The PZT disk theoretical and experimental steady-state temperatures for an input voltage of 50 V and the modes identified by impedance lows (Fig. 6) are presented in Table 3. To ensure steady-state temperatures, the actuator was driven for 10 min before measuring its surface temperature.

For those frequencies not matching the radial resonance frequency of the actuator, the theoretical model predicts the actuator temperature with a maximum error of 20%. When actuated at the radial ultrasonic resonance frequency of the PZT disk (28.5 kHz), mechanical strains in the PZT material increase. Internal friction in the PZT material generates heat energy not fully captured in the theoretical model. Errors of up to 65% are recorded when the PZT disk is driven at its resonance frequency and with an input voltage of 50 V. Despite the large errors between the predicted and experimental temperatures at the radial frequency of the actuator, the disk remained at a negative temperature when a sinusoidal input signal of 50 V was applied. It can be concluded that the actuator rise in temperature does not contribute to ice-interface melting due to heat propagation.

An actuator configuration such that higher voltages to the actuator would be required (for similar or lower impedance values) would imply an increase in the dissipated power, P_p, and therefore also increase the actuator temperature. If the actuator temperature exceeded freezing, there would be uncertainties during experimental correlations between ice delamination and transverse shear stress predictions, since thermal energy could be the main factor debonding the ice layer.

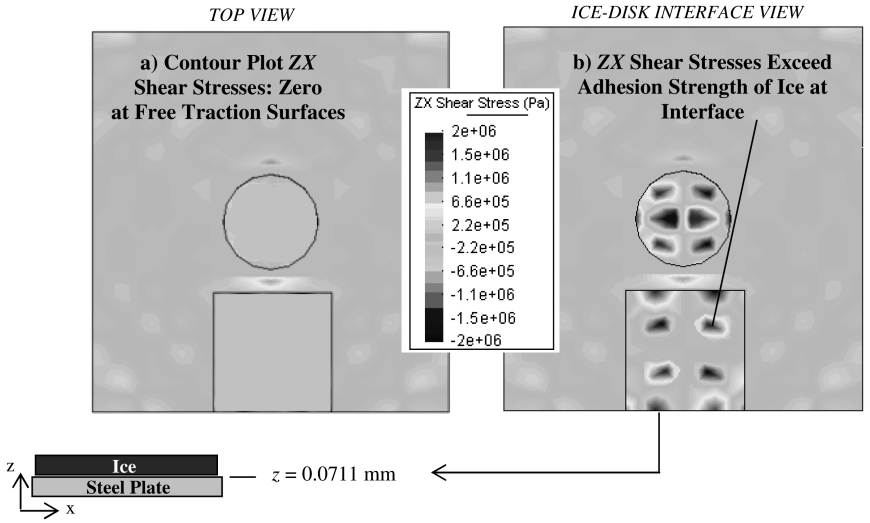

Fig. 8 Left: Top view of transverse shear stresses of the steel plate, PZT actuator, and ice layer. Right: *ZX* transverse shear stresses at the ice-layer interface (60 W input power, 28.5 kHz radial mode).

Table 3 Temperature of a 2.54-mm-thick PZT-4 disk actuator attached to 0.71-mm-thick Steel plate. environment temperature −10°C

Frequency, kHz	Impedance, Ω	Max. theor temp, °C	Exp temp, °C	% error
18	480	−9.0	−9.1	1%
28.5	65	−8.4	−3	65%
33	70	−8.5	−6.8	20%
37	56	−8.3	−6.9	17%

IV. Experimental Results

A. Instantaneous Ultrasonic Delamination of Freezer Ice

As presented in Fig. 9, the predicted voltage amplitude required for the PZT-4 disk actuator to generate interface transverse shear stresses on a 2.5-mm-thick ice layer that exceed the shear adhesion strength of ice to steel (1.5 MPa) is approximately 50 V (28.5 kHz actuator radial mode). Ice debonding is predicted when 28.5 kHz and 50 V are applied to the disk actuator.

A 2.5-mm-thick ice layer was allowed to accrete to the surface of the steel plate for 5 h at a temperature of −20°C. The steel plate was placed vertically so gravity forces would clearly show the ice falling after delamination. The actuator was excited at its radial resonance (28.5 kHz), and accreted ice was instantaneously removed for input voltages exceeding 43 V. Thus, the ultrasonic shear de-icing method is experimentally validated. Thermocouples placed on both the actuator and the steel plate showed temperatures of −18°C at the instant of ice debonding, eliminating any concern of delamination due to thermal propagation.

The actuator power consumption required to debond the freezer ice layer was measured to be 50 W or 0.077 W/cm^2 (0.5 $W/in.^2$).

B. Effects of Ice Thickness on Ultrasonic De-Icing

During this research, it was predicted that the designed ultrasonic actuation would delaminate layers as thin as 2.5 mm. This ice thickness was the targeted minimum thickness to promote ice debonding. During experimental testing, three ice thicknesses were tested: a thickness in the range of 2.5 mm, a thickness smaller than 2.5 mm by approximately 30%, and a thickness larger than 2.5 mm by approximately 30%. The three ice layers of different thicknesses froze on the surface of the 30.5 cm × 30.5 cm stainless steel plate at a temperature of −20°C. A schematic of the three different ice thickness layers (1.77,2.28, and 3.81 mm) is shown in Fig. 10. The actuator, steel plate, and accreted-ice-layer system were modeled using finite element analysis described above.

The *XY* shear stresses at the interface of the ice layers were calculated for the maximum of the sinusoidal input voltage (50 V).

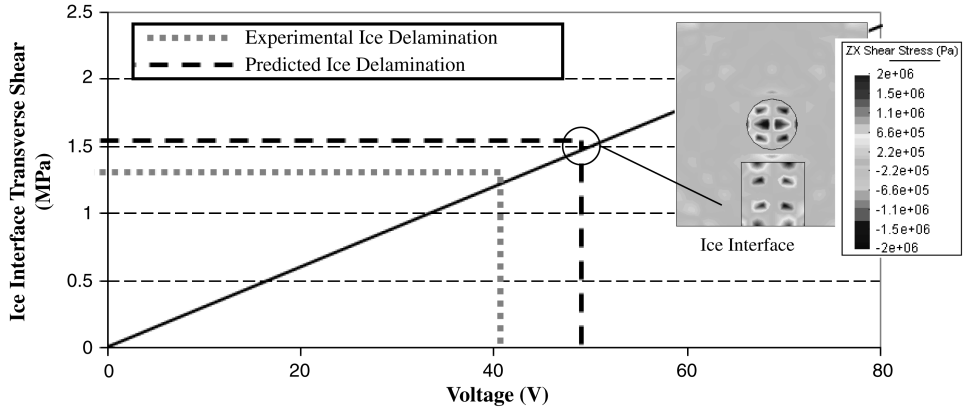

Fig. 9 Predicted transverse shear stress vs applied voltage at the interface of a 2.54-mm-thick ice layer on a 0.71 mm steel plate driven by a 38.1-mm-radius 2.54-mm-thick PZT-4 Disk (28.5 kHz).

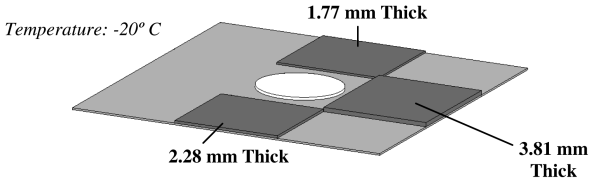

Fig. 10 Schematic of 30.5 cm × 30.5 cm steel plate with ice layers of 1.77, 2.28, and 3.81 mm thickness.

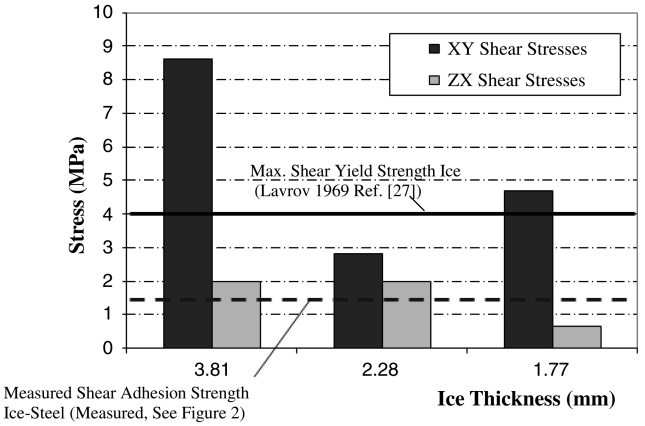

Fig. 11 *XY* and *ZX* shear stress for ice layers of 3.81-, 2.28-, and 1.77-mm-thick ice debonding is predicted for the 3.81- and 2.28-mm-thick layers, while cracking is expected for the 2.28- and 1.77-mm-thick layers. The 1.77-mm-thick ice layer is predicted to not debond when 50 V, 28.5 kHz signal input.

These shear stresses are responsible for ice cracking, but not debonding. Debonding processes are due to *ZX* transverse shear stresses. A comparison of the *XY* shear stresses and the *ZX* shear stresses when the disk actuator is driven at 28.5 kHz and 50 V amplitude sinusoidal input is depicted in Fig. 11. The thinnest ice layer (1.77-mm-thick) experiences average *XY* shear stress values as compared with the other two ice thickness layers. The 1.77-mm-thick ice layer also experiences the lowest theoretical *ZX* transverse shear stresses concentration. Experimental results show that this ice layer (1.77 mm) does not completely delaminate instantaneously. The 1.77 mm layer also presents a larger crack distribution than the 2.28- and 3.81-mm-thick ice layers. This is due to the effects of *XY* shear stresses, and because the patch remains bonded to the host structure, since the *ZX* stresses are not large enough to immediately delaminate the ice patch. A snapshot of the ice layers after the actuator was turned on is presented in Fig. 12.

The 2.28 and the 3.81 mm ice layers delaminate instantaneously when the PZT disk is actuated at its radial ultrasonic resonance and with an input power of 50 W. These experimental results corroborate the hypothesis that transverse shear stresses generated by continuous ultrasonic vibration are responsible for ice delamination, while *XY* shear stresses contribute to ice cracking. They also show, as predicted, that thicker ice layers undergo larger concentrations of *ZX* transverse shear stresses.

C. Ultrasonic De-Icing of Airfoil-Shaped Structures

1. Finite Element Modeling

Upon demonstrating instantaneous ice delamination due to ultrasonic transverse shear stresses on steel plates, work efforts focused on using this approach to remove thin freezer ice layers from a more complex structure representative of a rotor blade leading edge. An airfoil-shaped structure was fabricated out of 0.7-mm-thick steel.

The airfoil-shaped structure was modeled using the finite elements methods previously presented. Two freezer ice patches (2 mm× 23 mm × 95 mm) accreted to the top surface of the leading edge of the airfoil-shaped structure were modeled as being perfectly bonded to the structure. The transverse shear stresses created at the interface of the accreted ice layers were predicted. These ultrasonic transverse shear stresses were generated by two PZT-4 disk actuators of 2.54 mm thickness and 38 mm radius. A schematic and finite elements used to model the system are shown presented in Fig. 13.

The predicted ultrasonic frequencies best suited to generate transverse shear stresses able to instantaneously debond accreted ice would be those providing minimum impedance values, as shown in Fig. 14. It is at these frequencies (28.5 and 30.5 kHz) that the ice-interface transverse shear stress is maximized for a given input voltage. Note that at those frequencies away from impedance lows, the ice-interface transverse shear stresses are well under the adhesion strength of ice to steel (1.5 MPa) for the given input voltage (100 V). At those frequencies, ice delamination is not predicted.

To promote ice delamination at frequencies not coinciding with ultrasonic modes, an increase in input voltage would be required (500 V for the 23 kHz mode and 375 V for the 33.5 kHz mode). Even though there is an increase in required input voltage to provide stresses able to delaminate the accreted ice layer, the related power

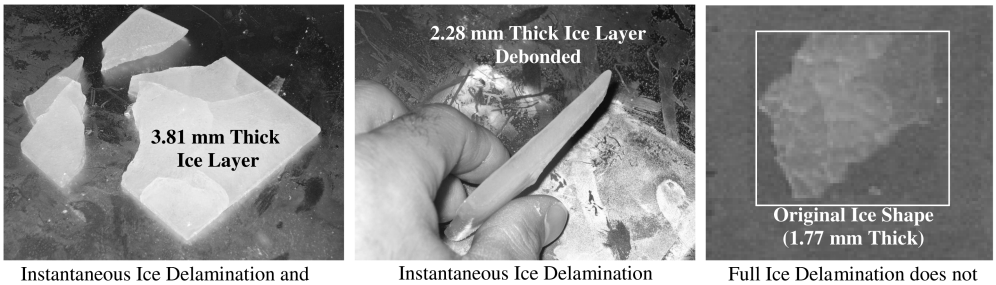

Instantaneous Ice Delamination and Cracking | Instantaneous Ice Delamination | Full Ice Delamination does not Occurred. Cracking is Observed

Fig. 12 Experimental ice debonding and fracture patterns under ultrasonic *ZX* and *XY* shear stresses (28.5 kHz, 50 V, −20°C). Patterns agree with finite element method predictions.

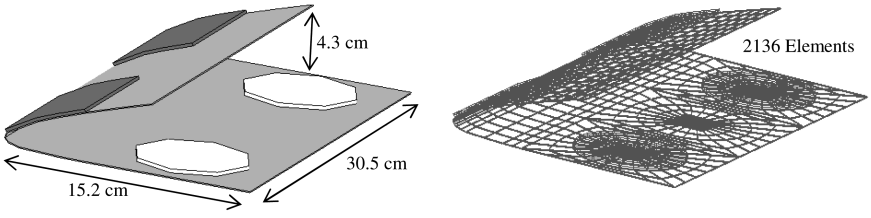

Fig. 13 Schematic and finite elements used to model the airfoil-shaped structure with accreted ice layers and PZT actuators.

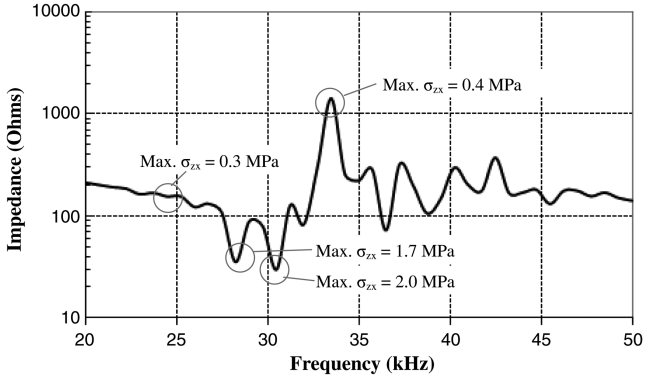

Fig. 14 Predicted impedance for airfoil-shaped structure with two disk actuators and two 3-mm-thick accreted freezer ice layers. Impedance low ultrasonic modes (28.5 and 30.5 kHz) are suitable for de-icing.

would decrease for an antiresonance mode, as shown in Fig. 15. These results assume that impedance matching between the load and the driving electronics is enforced. The low-power antiresonance mode (33.5 kHz) could not be triggered, since the impedance of this mode exceeded the matching network impedances. For this reason, resonance ultrasonic modes (28.5 and 30.5 kHz) are selected as candidates for experimental correlation with predicted ice-interface transverse shear stress values.

Modeling of the ice-interface transverse shear stresses generated when the ultrasonic actuator is excited at its impedance lows are presented in Fig. 16. Both ultrasonic modes provide transverse shear stresses exceeding the adhesion strength of ice when 100 V are applied.

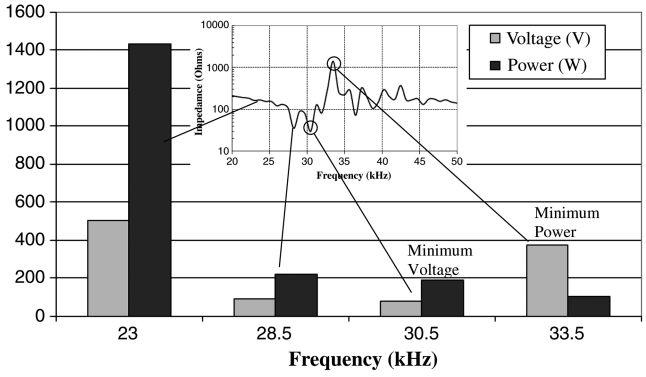

Fig. 15 Power and voltage requirements to reach transverse shear stresses of 1.5 MPa at the ice interface of freezer ice (3-mm-thick) accreted to a steel airfoil-shaped structure.

2. *Experimental Correlation*

Two ultrasonic disk actuators were bonded to the bottom of a steel airfoil-shaped structure of same dimensions as the one shown in Fig. 13. Two ice patches (∼3 m thick) were frozen on the top surface at a temperature of −20°C.

In this set of experiments, the actuators were excited at 28 and 30.5 kHz ultrasonic modes, respectively, (200 W input power). These two ultrasonic modes were selected because the impedance of the system was in the range of the available impedance matching networks. The ultrasonic excitation provided localized ice-interface stresses exceeding the adhesion strength of ice to steel. These stresses weakened the ice locally and instantaneous ice delamination was observed at certain locations of the ice patch. Subsequent complete ice delamination occurred ∼2 s later for both ultrasonic modes. Ice delamination was not observed when 200 W were applied at frequencies corresponding to ultrasonic modes not matching the resonance of the actuator. These experimental results demonstrate the potential use of ultrasonic excitation in high curvature areas such as helicopter leading-edge protection caps.

V. Conclusions

Based on the results obtained during the investigation of ultrasonic de-icing actuators and their effects on freezer ice, the following conclusions are made:

1) It was predicted and validated experimentally that instantaneous delamination between ice and isotropic plates representative of helicopter leading-edge protection caps is possible using ultrasonic excitation (27 kHz–32 kHz), as transverse shear stresses generated at the ice interface exceed the adhesion strength of the ice.

2) In the presented cases, instantaneous ice delamination is not due to thermal processes related to ultrasonic vibration, as the PZT material remained well under freezing temperatures at the moment of ice debonding.

3) The power required to instantaneously debond freezer ice layers (ranging between 2 mm and 4 mm in thickness) accreted to a 0.7-mm-thick steel plate was measured to be 0.05 W/cm^2 (0.34 W/in^2).

4) Impedance matching between the load (actuator) and driving electronics enhances instantaneous ice delamination using piezoelectric actuators, since this condition maximizes input power conversion into mechanical ice debonding stresses.

5) Ultrasonic ice-interface transverse shear stresses can be predicted using finite element methods that model the actuator, host structure and accreted ice layer.

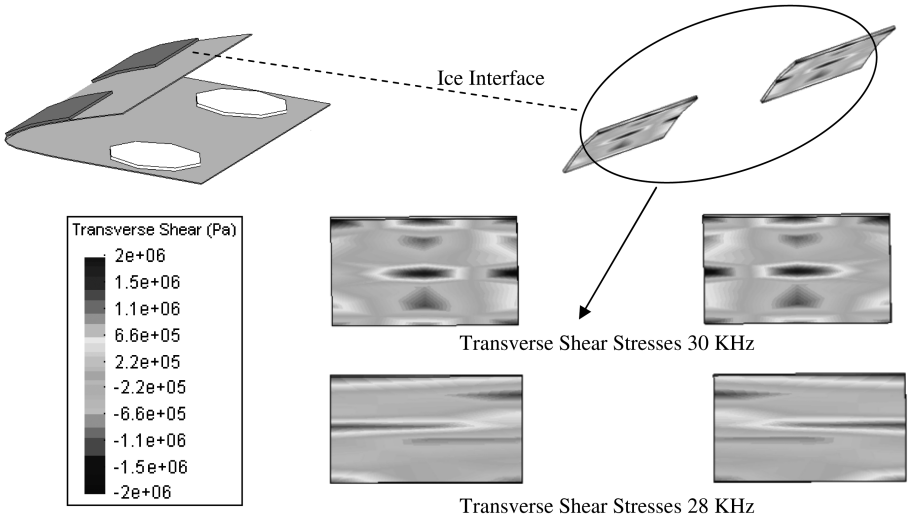

Fig. 16 Predicted ultrasonic transverse shear stresses at the ice interface of freezer ice accreted to an airfoil-shaped structure (100 V). Transverse shear stresses exceed the adhesion shear strength of freezer ice to steel.

6) Ice-interface transverse shear stresses are dependent on the accreted ice thickness. At a constant actuation input, thicker ice layers undergo larger transverse shear stresses. A 50 W ultrasonic excitation input provided by a 2.5-mm-thick, 7.6-cm-diam PZT-4 disk (28.5 kHz radial resonance frequency) is able to instantaneously debond freezer ice layers as thin as 2 mm.

7) Freezer ice formed on an airfoil-shaped isotropic structure can also be removed by ultrasonic excitation that provides interface transverse shear stresses exceeding the adhesion strength of the ice to the substrate. The required input power and actuator density had to be increased with respect to plate configurations due to the higher structure stiffness of the airfoil shape configuration (0.2 W/cm^2, 1.4 $W/in.^2$).

Studies on the effect of ultrasonic excitation on *impact icing* are suggested to further demonstrate the ability of ultrasonic excitation to de-ice realistic helicopter blade structures under icing conditions.

Acknowledgments

The authors would like to thank Bell Helicopters, a Textron Company, and the U.S. Army for sponsoring this research. This research is partially funded by the Government under agreement no. W911W6-06-2-0008 and by FBS Worldwide, Inc. Thanks to Aviation Applied Technology Directorate Phase I Small Business Innovation Research contract no. W911W6-08-C-0019. The views and conclusions contained in this document are those of the authors and should not be interpreted as representing the official policies, either expressed or implied, of the U.S. Government.

References

[1] Gent, R. W., Dart, N. P., and Candsdale, J. T., "Aircraft Icing," *Philosophical Transactions of the Royal Society of London, Series A: Mathematical and Physical Sciences*, Vol. 358, 2000, pp. 2873–2911. doi:10.1098/rsta.2000.0689

[2] Coffman, H. J., "Helicopter Rotor Icing Protection Methods," *Journal of the American Helicopter Society*, Vol. 32, No. 2, April 1987, pp. 34–39. doi:10.4050/JAHS.32.34

[3] Scavuzzo, R. J., Chu M. L, and Kellackey, C. J., "Impact Ice Stress in Rotating Airfoils," *Journal of Aircraft*, Vol. 28, No. 7, July 1991, pp. 450–455. doi:10.2514/3.46048

[4] Zumwalt, G. W., "Icing Tunnel Tests of Electro-Impulse De-icing of Engine Inlet and High-Speed Wings," 23rd Aerospace Sciences Meeting, AIAA Paper 83-2529, Reno, NV, Jan. 1985.

[5] Reinmann, J. J., Shaw, R. J., and Ranaudo, R. J., "NASA's Program on Icing Research and Technology," *Proceedings of the Symposium on Flight in Adverse Environmental Conditions*, Kluwer, Norwell, MA, May 1989, pp. 73–78.

[6] Martin, C. A., and Putt, J. C., "Advanced Pneumatic Impulse Ice Protection System (PIIP) for Aircraft," *Journal of Aircraft*, Vol. 29, No. 4, 1992, pp. 714–716. doi:10.2514/3.46227

[7] Venna, S. V., Lin, Y., and Botura, G., "Piezoelectric Transducer Actuated Leading Edge De-Icing with Simultaneous Shear and Impulse Forces," *Journal of Aircraft*, Vol. 44, No. 2, March–April 2007, pp. 510–515.

[8] Palacios, J. L., and Smith, E. C., "Dynamic Analysis and Experimental Testing of Thin-Walled Structures Driven By Shear Tube Actuators," 46th AIAA/ASME/ASCE/AHS/ ASC Structures, Structural Dynamics & Materials, AIAA Paper 2005-2112, Austin, TX, April 2005, pp. 3862–3875.

[9] Ramanathan, S., Varadhan, V. V., and Varadhan, V. K., "De-Icing of Helicopter Blades Using Piezoelectric Actuators," *Smart Structures and Materials 2000: Smart Electronics and MEMS*, SPIE, Bellingham, WA, March 2002, pp. 354–363.

[10] Palacios, J., Smith, E., Rose, J., and Gao, H., "Ultrasonic Shear Wave Anti-Icing System for Helicopter Rotor Blades," *62nd Annual Forum Proceedings—American Helicopter Society*, AHS International, Alexandria, VA, May 2006, pp. 1492–1502.

[11] Lemont, H. E., and Upton, H., "Vibratory Ice Protection for Helicopter Rotor Blades," U.S. Army Air Mobility Research and Development Lab., TR-77-29, June 1978.

[12] Chu, M. C., and Scavuzzo, R. J., "Adhesive Shear Strength of Impact Ice," *AIAA Journal*, Vol. 29, No. 11, Nov. 1991, pp. 1921–1926. doi:10.2514/3.10819

[13] Bascom W., Cottington R., and Singleterry, C., "Ice Adhesion to Hydrophilic and Hydrophobic Surfaces," *Journal of Adhesion Science and Technology*, Vol. 1, Oct. 1969, pp. 246–263.

[14] Raraty, L., and Tabor, A., "The Adhesion and Strength Properties of Ice," *Proceedings of the Royal Society of London, Series A: Mathematical and Physical Sciences*, Vol. 245, No. 1241, June 1958, pp. 184–201. doi:10.1098/rspa.1958.0076

[15] Stallabrass, J., and Price, R., "On the Adhesion of Ice to Various Materials," National Research Council Canada, Ottawa, July 1962, pp. 199–219.

[16] Jellinek, H., "Adhesive Properties of Ice," U.S. Army Corps of Engineers, Snow, Ice, and Permafrost Research Establishment, Rept. 38, Wilmette, IL, 1957.

[17] Someda, C., *Electromagnetic Waves*, Chapman and Hall, London, 1998, pp. 284–295.

[18] Jones, R., *Mechanics of Composite Materials*, Taylor and Francis, Philadelphia, 1999, pp. 345–356.

[19] Sirohi, J., and Chopra, I., "Fundamental Understanding of Piezoelectric Strain Sensors," *Journal of Intelligent Material Systems and Structures*, Vol. 11, No. 4, April 2000, pp. 246–257.

[20] Jarng, S., "Comparison of Barrel-Stave Sonar Transducer Simulation Between a Coupled FE-BEM and ATILA," *IEEE Sensors Journal*, Vol. 3, No. 4, 2003, pp. 439–446. doi:10.1109/JSEN.2003.815846

[21] Uchino, K., *FEM and Micromechatronics with ATILA Software*, CRC/ Taylor & Francis, Philadelphia, May 2008.

[22] "ATILA Finite Element Analysis for Piezoelectric and Magnetostrictive Structures Version 5.3. User's Manual," Institut Supérieur d'Electronique du Nord, Lille, France, July 2005, pp. 35–38.

[23] Safari, A., and Akdogan, E. K., *Piezoelectric and Acoustic Materials for Transducer Applications*, Springer, New York, 2008, pp. 241–257, Chap. 12.

[24] Zhou, S., Liang, C., and Rogers, A., "Integration and Design of Piezoelectric Elements in Intelligent Structures," *Journal of Intelligent Material Systems and Structures*, Vol. 6, Nov. 1995, pp. 733–743. doi:10.1177/1045389X9500600601

[25] Lavrov, V., "Load-Deformation of Ice," *Zhurnal Tekhnicheskoi Fiziki*, Vol. 32, No. 1, Jan. 1962, pp. 101–105.

N. Wereley
Associate Editor